Journal of Materials Research and Technology 41 (2026) 3101–3106

Contents lists available at ScienceDirect

Journal of Materials Research and Technology

journal homepage: www.elsevier.com/locate/jmrt

# Anisotropic elastic properties in glass, aramid, and carbon fibers

Kimiyoshi Naito [a,b,*], Chiemi Nagai [a], Keiichi Shirasu [a,c]

[a] National Institute for Materials Science (NIMS), Research Center for Structural Materials, Polymer Matrix Composites Group, 1-2-1 Sengen, Tsukuba, Ibaraki, 305-0047, Japan
[b] Tohoku University, Department of Aerospace Engineering 6-6-01 Aza-Aoba, Aramaki, Aoba-ku, Sendai, Miyagi, 980-8579, Japan
[c] Tohoku University, Department of Finemechanics, 6-6-01, Aza-Aoba, Aramaki, Aoba-ku, Sendai, Miyagi, 980-8579, Japan

ARTICLE INFO

*Keywords:*
Fiber
Polymer-matrix composites (PMCs)
Nanoindentation
Anisotropy
Elastic constants

ABSTRACT

Fibers used in fiber-reinforced polymer matrix composites (FRPs) exhibit significant anisotropy between radial and axial directions. In this study, six epoxy composites containing different fiber types—E-glass, aramid, and carbon fibers—were prepared. Nanoindentation tests were conducted on three orthogonal cross-sections of each fiber. The Vlassak–Nix (VN) model, based on theoretical implicit equations derived from anisotropic elasticity theory, was applied to extract five independent elastic constants: $c_{11}$, $c_{12}$, $c_{13}$, $c_{33}$, and $c_{44}$. The anisotropic index and its correlation with tensile modulus and extrapolated indentation modulus were systematically evaluated. Results revealed that fibers with higher stiffness exhibited greater anisotropy. These findings highlight the importance of considering both anisotropy and stiffness in fiber selection for composites and additive manufacturing applications.

## 1. Introduction

Fiber-reinforced polymer matrix composites (FRPs) are widely used in aerospace, automotive, and structural applications due to their high strength-to-weight ratios and customizable mechanical properties. These composites consist of reinforcing fibers embedded in a polymer matrix, where the mechanical performance is primarily governed by the properties and orientation of the fibers [1,2].

Commonly used fibers include E-glass, aramid (e.g., Kevlar), and PAN-based carbon fibers (e.g., T300), each offering distinct advantages in terms of stiffness, strength, and cost [3–5]. Ari [6] further demonstrates that composites reinforced with chopped glass, carbon, and aramid fibers significantly outperform unreinforced polymers in tensile, flexural, and impact resistance. While pseudo-isotropic in-plane orientation is rarely utilized [7], strategic fiber alignment is often employed to exploit anisotropy and enhance performance [8].

Accurate evaluation of strength, elasticity, and load-bearing capacity requires a thorough understanding of the anisotropic elastic properties imparted by the reinforcing fibers [9]. This directional mechanical behavior is critical for optimizing the structural integrity and functionality of FRPs.

The anisotropic elastic behavior of FRPs has been extensively studied due to its critical role in determining mechanical performance [10]. In the context of additive manufacturing, recent studies have highlighted the implications of fiber anisotropy in FRPs [11]. Parmiggiani et al. [12] examined the effects of fiber orientation on tensile and bending properties. To optimize mechanical performance, Soori et al. [13] proposed a topology optimization framework that integrates artificial intelligence (AI), machine learning (ML), and deep learning (DL) techniques. This method enables the design of components with spatially tailored anisotropic properties, maximizing structural efficiency.

The elasticity of fibers is often modeled as transversely isotropic, defined by five independent elastic constants: $c_{11}$, $c_{12}$, $c_{13}$, $c_{33}$, and $c_{44}$, where the fiber axis corresponds to the 3-direction [14,15]. This anisotropy is especially relevant in load-bearing applications. Nanoindentation has become a standard technique for localized mechanical characterization, particularly in anisotropic materials [16,17]. The Oliver and Pharr [18,19] method enables the determination of indentation modulus ($M$), and its extension through the Vlassak–Nix (VN) [20,21] model incorporates directional cosines and elastic tensors to account for anisotropy. Shirasu et al. [22,23] applied nanoindentation to PAN- and pitch-based carbon fibers, revealing significant differences in axial and radial moduli. Pitch-based fibers exhibited a modulus anisotropy ratio ($E_f/E_T$) of approximately 165, compared to 11 for PAN-based

* Corresponding author. National Institute for Materials Science (NIMS), Research Center for Structural Materials, Polymer Matrix Composites Group, 1-2-1 Sengen, Tsukuba, Ibaraki, 305-0047, Japan.
*E-mail address:* NAITO.Kimiyoshi@nims.go.jp (K. Naito).

https://doi.org/10.1016/j.jmrt.2026.01.225
Received 5 October 2025; Received in revised form 18 January 2026; Accepted 29 January 2026
Available online 30 January 2026

fibers, reflecting their highly crystalline microstructure. FEA has been employed to simulate indentation behavior and validate experimental results. Goto et al. [24] demonstrated that mesh resolution and integration parameters significantly affect the accuracy of modulus predictions, with the VN model tending to overestimate values at small tilt angles unless finely discretized. To bridge microstructural and macroscopic property evaluation, Gonabadi et al. [25] proposed a hybrid methodology combining nanoindentation with inverse FEA to extract orthotropic engineering constants from 3D-printed composites. This approach enables accurate stiffness characterization without extensive mechanical testing. Despite these advancements, the anisotropic elastic properties of commonly used fibers—such as glass, aramid, and T300 PAN-based carbon fibers—remain insufficiently characterized [26,27].

Accurate evaluation of the elastic properties of individual fibers is essential for predicting the mechanical behavior of FRPs. Traditional macroscopic testing methods are limited in resolving the directional properties of microscale fibers. Nanoindentation has emerged as a powerful technique for characterizing local mechanical properties, particularly in anisotropic materials [16,17].

The novelty of this study lies in the systematic evaluation of five elastic constants using nanoindentation and VN modeling across a range of fiber types, and the establishment of a quantitative correlation between anisotropy and stiffness, which has not been previously reported in such breadth.

The objective of this study is to extract five independent elastic constants from nanoindentation data for various fiber types and to evaluate the correlation between anisotropy and stiffness, thereby informing fiber selection for advanced FRP applications.

## 2. Experimental procedure

### 2.1. Materials

The E-glass fiber used in this study was an alumino-borosilicate glass fiber with less than 1 % w/w alkali oxides, supplied from Nippon Electric Glass Co., Ltd., Shiga, Japan. The aramid fibers—Kevlar29, Kevlar49, Kevlar119, and Kevlar129—were poly-(para-phenylene terephthalamide) (PPTA) fibers provided by DuPond-Toray Co., Ltd., Tokyo, Japan. The T300 high strength PAN-based carbon fiber was obtained from Toray Industries, Inc., Tokyo, Japan. The diameter ($d_f$), density ($\rho_f$), and Young's modulus ($E_f$) for each fiber are summarized in Table 1.

### 2.2. Specimen preparation

To prepare the longitudinal (0°), 45°, and transversal (90°) cross-sections for nanoindentation testing, FRP samples were fabricated using +45°/0°/-45°/90° symmetric layups for E-glass and T300 fibers (via prepreg), and epoxy impregnated fiber bundles for aramid fibers. The samples were embedded in epoxy resin and polished using an automatic polishing machine (Automet 2000, Buhler Ltd., Saitama, Japan), followed by polycrystalline diamond suspensions of 6 μm and 3 μm, as shown in Fig. 1. The cross-sections were observed using a scanning probe microscope (SPM) (SPM-9700, Shimadzu Corp., Kyoto, Japan) to confirm fiber orientation and surface quality.

### 2.3. Nanoindentation test

Nanoindentation tests were performed on the longitudinal (0°), 45°, and transversal (90°) cross-sections of each fiber using a Hysitron TriboScope (Bruker Corp., Tokyo, Japan) equipped with a standard diamond Berkovich indenter (TI-0039). The indenter had a half angle of 65.27° and an included angle of 142.30°.

Loading and unloading times were set to 20 s each, with a 2 s holding period. The maximum indentation depth was adjusted for each fiber type to maintain a contact depth between 80 and 160 nm.

On the transversal (90°) and 45°cross-sections, indentation tests were made at the center of the fiber. On the longitudinal (0°) cross-section, fibers with minimal inclination were selected for testing.

The indentation modulus was calculated using the Oliver-Pharr method [18,19,26,27]. The indenter tip was calibrated on a quartz standard. The Young's modulus and Poisson's ratio of the diamond tip were $E_i = 1140$ GPa and $\nu_i = 0.07$, respectively.

The tilt angle $\alpha$ of the fiber was estimated from the elliptical shape of

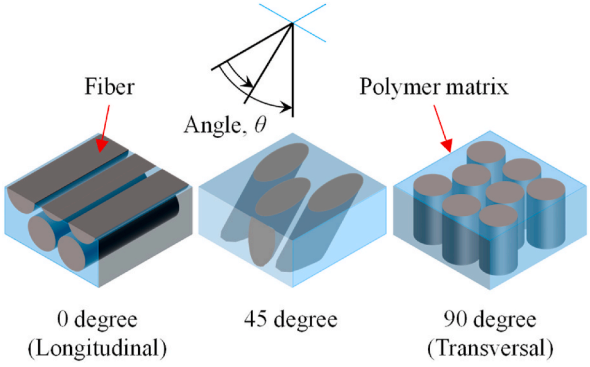


**Fig. 1.** Schematic view of anisotropy nanoindentation testing sample.

**Table 1**
Measured properties of the glass, aramid, and carbon fibers, including the diameter ($d_f$), density ($\rho_f$), Young's modulus ($E_f$), measured indentation moduli ($M_A$, $M_{45}$, and $M_R$) obtained from nanoindentation tests carried out on transversal (90°), 45°, and longitudinal (0°) cross-sections of fibers, calculated extrapolated indentation modulus at $\alpha = 0°$ ($M_{A0}$), and elastic constants ($c_{11}$, $c_{12}$, $c_{13}$, $c_{33}$, and $c_{44}$).

| | Glass | Aramid | | | | Carbon |
|---|---|---|---|---|---|---|
| | E-glass | Kevlar29 | Kevlar49 | Kevlar119 | Kevlar129 | T300 |
| $d_f$ (μm)[a] | 9.20 | 12.43 | 10.73 | 12.43 | 12.43 | 6.91 |
| $\rho_f$(g/cm$^3$)[a] | 2.54 | 1.44 | 1.45 | 1.44 | 1.44 | 1.76 |
| $E_f$ (GPa)[a] | 70 | 70.5 | 112.4 | 54.7 | 96.6 | 230 |
| $M_A$ (GPa) | 70.04 ± 3.08 | 20.59 ± 1.06 | 23.85 ± 1.28 | 16.53 ± 0.90 | 19.75 ± 1.16 | 66.26 ± 3.66 |
| $M_{45}$ (GPa) | 67.99 ± 2.15 | 12.78 ± 0.78 | 13.70 ± 0.91 | 11.02 ± 0.75 | 12.60 ± 1.00 | 27.67 ± 2.15 |
| $M_R$ (GPa) | 68.71 ± 1.61 | 7.93 ± 0.81 | 7.06 ± 0.58 | 7.08 ± 0.63 | 8.04 ± 0.41 | 16.08 ± 2.86 |
| $M_{A0}$ (GPa) | 70 | 24.5 | 28 | 20 | 23 | 82 |
| $c_{11}$ (GPa) | 75.65 | 8.97 | 8.60 | 8.18 | 9.93 | 13.77 |
| $c_{12}$ (GPa) | 18.91 | 0.52 | 0.40 | 0.52 | 0.51 | 3.41 |
| $c_{13}$ (GPa) | 18.91 | 2.85 | 2.70 | 2.61 | 3.13 | 3.42 |
| $c_{33}$ (GPa) | 75.65 | 72.21 | 114.02 | 56.26 | 98.48 | 231.36 |
| $c_{44}$ (GPa) | 28.37 | 2.47 | 1.93 | 2.12 | 1.47 | 9.64 |
| $A_L$ | 0 | 1.84 | 2.91 | 1.66 | 2.91 | 2.51 |

[a] Producer's data sheet, E-glass: catalog for E-glass in Japanese, 2025. Kevlar29, Kevlar49, Kevlar119, and Kevlar129: catalog for Kevlar in Japanese, 2025. T300: catalog for TORAYCA carbon fibers in Japanese, 2025.

the cross-section observed in SPM images. The major and minor radii were denoted as $R$ and $r$, respectively. Assuming the fiber is a perfect cylinder inclined at angle $\alpha$, the following geometric relationship was used:

$$\alpha = \cos^{-1}\left(\frac{r}{R}\right) \quad (1)$$

Note: Due to the irregular ellipsoidal shape of the T300 fiber cross-section, direct measurement of $\alpha$ was not feasible. Instead, average tilt angles from other fibers (10.4° and 43.6°) were used as proxies, assuming similar embedding and polishing conditions.

Over 20 indentations were performed per orientation to obtain statistically reliable modulus values ($M_A$, $M_{45}$ and $M_R$).

The elastic moduli of anisotropic material are dependent on crystallographic orientation. Delafargue and Ulm [28] derived closed-form equations for $M$ based on the elastic constants when the longitudinal (0°) and transverse (90°) directions of the fibers were used as the indentation axis ($M_L$ and $M_T$): Vlassak and Nix [20,21] and Swadener and Pharr [29] proposed theoretical implicit equations (VN model) for the indentation-derived elastic modulus.

The VN model, based on theoretical implicit equations derived from anisotropic elasticity theory, was used to calculate indentation-derived elastic moduli as a function of fiber tilt angle. The five elastic constants ($c_{11}$, $c_{12}$, $c_{13}$, $c_{33}$, and $c_{44}$) were extracted by fitting the VN model to the experimental data.

Due to the geometric constraints of fiber cross-sections and the difficulty in precisely controlling tilt angles during sample preparation, additional experimental tilt angles were not feasible. The VN model was therefore used to interpolate modulus values between the measured orientations.

## 3. Results and discussion

### 3.1. Morphology

Following specimen preparation, the morphology of the fiber cross-sections was examined using SPM. Fig. 2 shows representative images of the transversal (90°), 45°, and longitudinal (0°) sections of each fiber. E-glass fibers exhibited smooth circular, ellipsoidal, and rectangular shapes in the respective orientations. Aramid fibers showed similar geometries, with characteristic striped patterns observed in the longitudinal section, indicative of their fibrillar structure. T300 PAN-based carbon fibers displayed irregular ellipsoidal shape in the transversal section, complicating direct geometric analysis.

### 3.2. Load–displacement curve

To evaluate the mechanical response under indentation, load–displacement curves were obtained for each fiber type (Fig. 3). T300 carbon fibers exhibited minimal hysteresis, with unloading curves returning near the origin, indicating predominantly elastic deformation. In contrast, E-glass and aramid fibers showed significant hysteresis and permanent plastic deformation, suggesting irreversible structural changes under the applied load. These observations are consistent with previous studies [17,22,23], confirming the elastic resilience of carbon fibers and the viscoplastic behavior of glass and aramid fibers. This indicates that these fibers underwent irreversible structural changes rather than purely elastic deformation [25,30].

The force needed to indent up to the selected maximum indentation depth in the fiber decreases with decreasing orientation angle from the transversal (90°) to longitudinal (0°) directions, indicating the reduction of the indentation modulus. The measured anisotropy in the indentation moduli of PAN-based carbon fibers is in agreement with previous nanoindentation studies on the same type of fibers [17,22,23,25,30].

### 3.3. Indentation modulus

To further quantify the anisotropic behavior observed in the load–displacement response, the orientation-dependent indentation modulus was analyzed. The average indentation moduli ($M_A$, $M_{45}$ and $M_R$) measured on the three cross-sections are summarized in Table 1. The results indicate a clear orientation dependence of the indentation modulus, particularly for aramid and carbon fibers. The tilt angles ($\alpha$) were estimated using Equation (1), with average values of 10.4° and 43.6° for the transversal and 45° sections, respectively. For T300 fibers, these average values were used due to the irregular cross-section shape.

Due to the irregular ellipsoidal shape of T300 fiber cross-sections, direct measurement of tilt angle was not feasible. Therefore, average

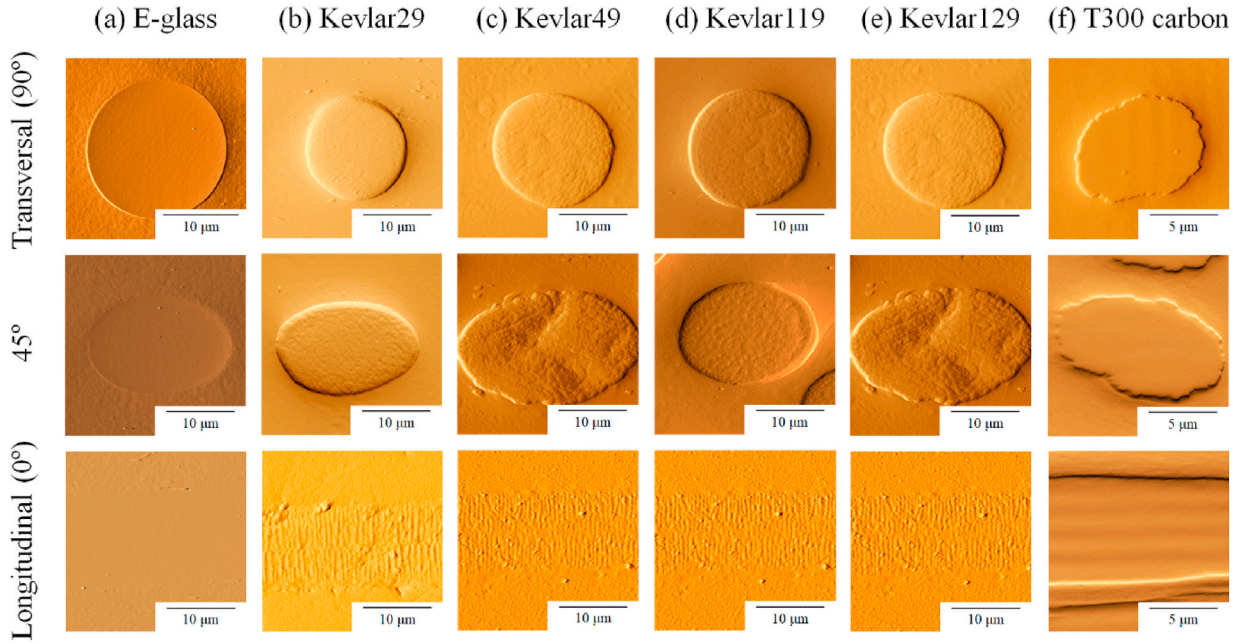


**Fig. 2.** SPM images of FRPs containing (a) E-glass, (b) Kevlar29, (c) Kevlar49, (d) Kevlar119, (e) Kevlar129, and (f) T300 carbon fibers. Each fiber is shown in transversal (90°), 45°, and longitudinal (0°) cross-sections.

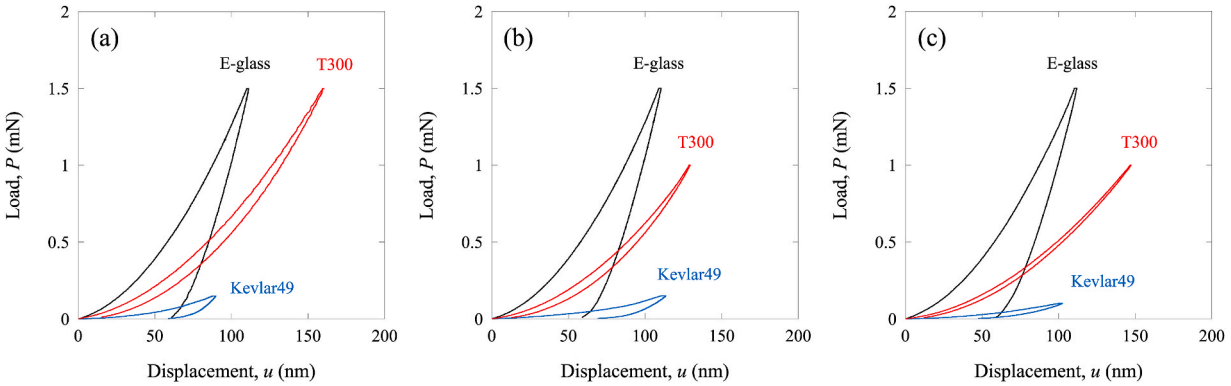


**Fig. 3.** Load-displacement curves of (a) transversal (90°), (b) 45° and (c) longitudinal (0°) cross-sections of fibers.

tilt angles from other fibers with similar preparation methods were used as a proxy, assuming comparable embedding and polishing conditions.

Fig. 4 shows the orientation dependence of the indentation modulus. The experimental data points are plotted alongside the VN model predictions. In brief, the extrapolated indentation modulus at $\alpha = 0°$ ($M_{A0}$) was deduced for each fiber type using the obtained indentation moduli ($M_A$, $M_{45}$ and $M_R$). Conversely, the five elastic constants ($c_{11}$, $c_{12}$, $c_{13}$, $c_{33}$, and $c_{44}$) were calculated analytically. Based on the obtained elastic constants, the indentation modulus was calculated by VN model using step sizes of 1° ($0° \leq \alpha < 10°$) and 5° ($10° \leq \alpha < 90°$). The deduced elastic constants for each fiber are indicated in Table 1. Note that $c_{66}$ was calculated by $c_{66} = (c_{11}–c_{12})/2$. E-glass fibers exhibited nearly constant modulus values across orientations, confirming their isotropic behavior. This isotropy is attributed to the amorphous microstructure of E-glass, which lacks long-range molecular orientation. In contrast, aramid and T300 carbon fibers showed a pronounced decrease in modulus with increasing tilt angle, particularly between 25° and 50°, beyond which the modulus plateaued. This behavior reflects the transversely isotropic nature of these fibers, where axial stiffness dominates. The change range in $M$ for T300 PAN-based carbon fiber was larger than that for aramid fiber.

The five elastic constants extracted using the VN model are listed in Table 1. The anisotropy index ($AL$) [31] was calculated for each fiber, with E-glass showing $AL = 0$, consistent with isotropy. High-modulus aramid fibers (Kevlar49, Kevlar129) and T300 carbon fibers exhibited higher $AL$ values, indicating strong anisotropy.

Fig. 5 presents the correlation between $AL$ and two stiffness parameters: tensile modulus ($E_f$) and extrapolated indentation modulus ($M_{A0}$). A clear positive correlation was observed in both cases, suggesting that fibers with higher stiffness tend to exhibit greater anisotropy.

For instance, K13D fibers, located in the upper right corner of both plots, showed the highest values for both $AL$ and modulus, reflecting their highly oriented graphitic structure and exceptional stiffness. In contrast, E-glass fiber, positioned in the lower left region, displayed low values for both parameters, was consistent with their amorphous and isotropic nature. The intermediate behavior of aramid fibers and T300 PAN-based carbon fibers suggested a semi-crystalline or turbostratic microstructure, which contributed to moderate anisotropy and stiffness, consistent with their balanced mechanical performance. This trend is consistent with previous findings [23], and can be attributed to the degree of molecular orientation and crystallinity. For example, pitch-based carbon fibers such as K13D exhibit highly aligned graphitic layers, resulting in extreme axial stiffness and anisotropy. Aramid fibers, with semi-crystalline regions and preferential chain alignment, show moderate anisotropy.

### 3.4. Implications for composite design

These results would underscore the importance of considering both anisotropic behavior and mechanical stiffness when selecting fibers for FRPs and additive manufacturing of FRPs. Sanei and Popescu [32] conducted a comprehensive review of 3D-printed FRPs. In this literature, Markforged Printers focused on 3D-printed composites, and the

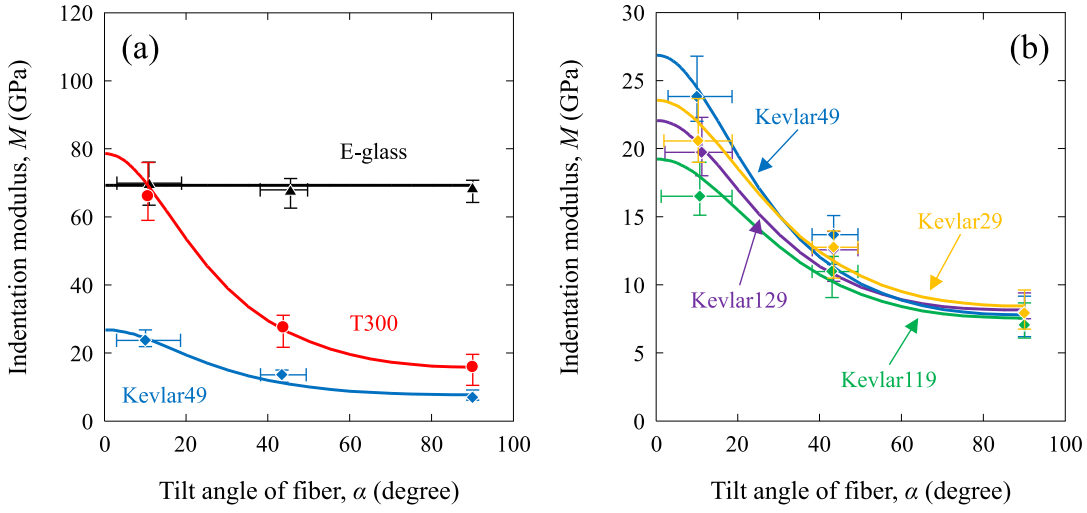


**Fig. 4.** Orientation dependence of the indentation modulus of fibers. (a) E-glass, aramid (Kevlar49), and T300 PAN-based carbon fibers, and (b) aramid (Kevlar29, Kevlar49, Kevlar119, and Kevlar129) fibers. The plotted data points and the solid lines represent the experimental results and VN-calculated results, respectively.

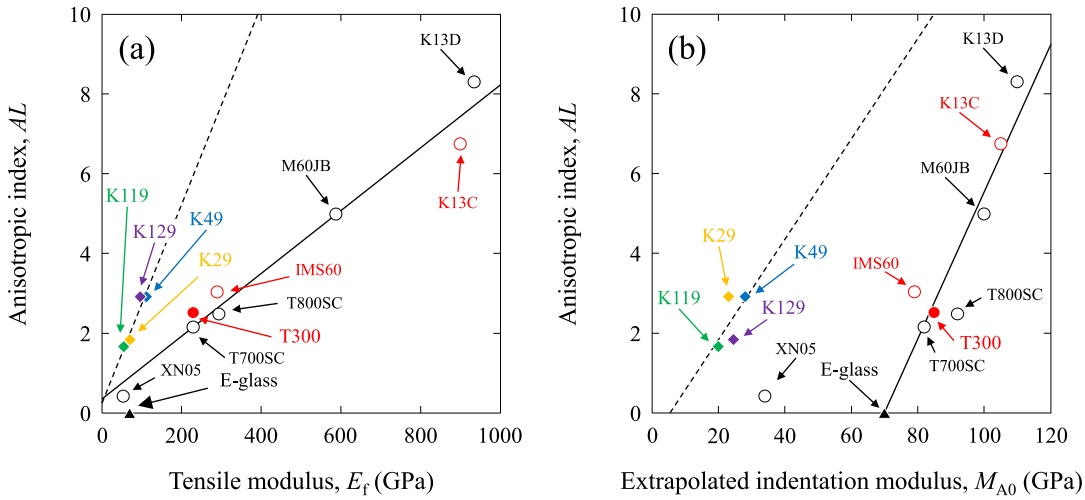


**Fig. 5.** Relationship between the anisotropic index and two mechanical properties—(a) tensile modulus and (b) extrapolated indentation modulus of E-glass (▲), aramid (◆), and T300 PAN-based carbon (●) fibers. ○ indicates other carbon fibers obtained from the previous investigation [23]. ○ indicates other carbon fibers obtained from this study.

fibers could only be used for the E-class-glass, Kevlar aramid, and T300-class carbon fibers. For example, the change in equivalent stiffness (50 % volume fraction of fiber, Young's modulus and Poisson's ratio of resin were 3 GPa and 0.33) using a micromechanics analysis [33] was calculated when the fiber orientation was changed for fibers (isotropic and anisotropic cases of E-glass, K29 aramid, T300 PAN-based, and K13D pitch-based carbon fibers).

To assess the impact of fiber anisotropy on composite performance, micromechanics analysis was conducted using a 50 % fiber volume fraction and resin properties of $E = 3$ GPa and $\nu = 0.33$. Fig. 6 shows the orientation dependence of the modulus difference (anisotropic vs. isotropic assumption) for composites reinforced with E-glass, Kevlar29, T300, and K13D fibers.

E-glass composites showed minimal variation with orientation, while aramid and carbon fiber composites exhibited significant reductions in stiffness at off-axis angles, particularly for highly anisotropic fibers.

These results underscore the importance of accounting for fiber anisotropy in composite design, especially for additive manufacturing applications where fiber orientation can vary spatially. The correlation between indentation-derived modulus and anisotropy further supports the use of nanoindentation as a reliable tool for evaluating fiber stiffness and orientation [34].

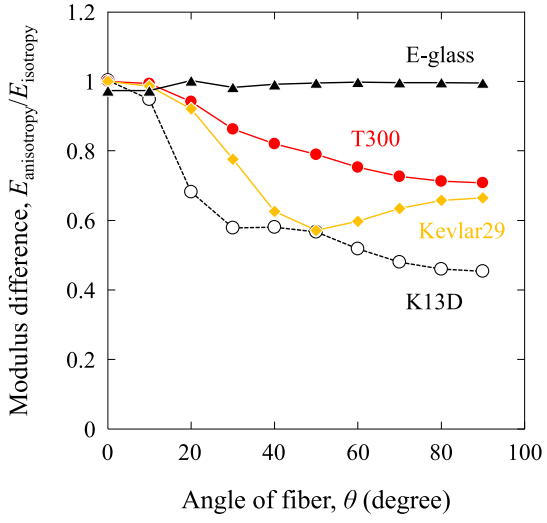


**Fig. 6.** Orientation dependence of the modulus difference of composites. The plotted data points represent the calculating results of E-glass, K29 aramid, T300 PAN-based, and K13D pitch-based carbon fibers composites, respectively.

### 3.5. Limitations

Several limitations should be noted. First, the estimation of fiber tilt angle ($\alpha$) is subject to error due to polishing-induced misalignment and cross-sectional irregularities. Second, surface roughness may affect indentation accuracy, particularly at shallow depths. Third, the indentation depth was limited to 80–160 nm to avoid substrate effects, but this may still influence the measured modulus depending on fiber diameter and local heterogeneity. Future studies should explore advanced imaging and alignment techniques to improve tilt angle accuracy and consider depth-dependent modulus analysis.

Although additional tilt angles would enhance the resolution of the orientation dependence, the current dataset, combined with VN modeling, provides sufficient accuracy for extracting elastic constants and evaluating anisotropy trends.

## 4. Conclusions

The elastic constants of glass, aramid, and carbon fibers embedded in epoxy composites were evaluated using nanoindentation combined with the VN model. Five independent elastic constants ($c_{11}$, $c_{12}$, $c_{13}$, $c_{33}$, and $c_{44}$) were successfully extracted for each fiber type by accounting for fiber tilt angles during indentation. Load–displacement curves revealed distinct deformation behaviors: T300 PAN-based carbon fibers exhibited predominantly elastic responses, while E-glass and aramid fibers showed significant plastic deformation. The orientation dependence of indentation modulus further emphasized the anisotropic mechanical response of aramid and carbon fibers, in contrast to the isotropic behavior of E-glass fibers. A clear positive correlation was observed between the anisotropy index (*AL*) and both tensile modulus and extrapolated indentation modulus. This trend reflects the influence of molecular orientation and microstructure on fiber stiffness and anisotropy. High-modulus aramid and carbon fibers exhibited strong anisotropy, while low-modulus aramid fibers were more isotropic.

These findings provide valuable insights for the design of fiber-reinforced composites, particularly in additive manufacturing where fiber orientation varies spatially. The demonstrated correlation between indentation-derived modulus and anisotropy validates nanoindentation as a reliable technique for evaluating fiber stiffness and orientation. This study is novel in its comprehensive application of nanoindentation and

VN modeling across multiple fiber types, and in establishing a quantitative framework linking stiffness and anisotropy for composite design.

## Authors' contributions

Kimiyoshi Naito: Conceptualization, Data curation, Formal analysis, Funding acquisition, Investigation, Methodology, Project administration, Resources, Software, Supervision, Validation, Visualization, Writing—original draft, Writing—review and editing. Chiemi Nagai: Data curation, Formal analysis, Investigation, Software, Validation, Visualization, Writing—review and editing. Keiichi Shirasu: Data curation, Investigation, Methodology, Supervision, Validation, Writing—review and editing. All the authors read and approved the manuscript.

## Funding

This work was supported by Japan science and technology agency (JST) K Program Grant Number JPMJKP24W1, Japan.

## Declaration of competing interest

The authors declare the following financial interests/personal relationships which may be considered as potential competing interests: Kimiyoshi Naito reports financial support was provided by National Institute for Materials Science. If there are other authors, they declare that they have no known competing financial interests or personal relationships that could have appeared to influence the work reported in this paper.

## Data availability

The datasets supporting the conclusions of this article are included within the article.

## References

[1] Zheng H, Zhu S, Chen L, Wang L, Zhang H, Wang P, Sun K, Wang H, Liu C. 3D printing continuous fiber reinforced polymers: a review of material selection, process, and mechanics-function integration for targeted applications. Polymers 2025;17(12):1601. https://doi.org/10.3390/polym17121601.

[2] Kurtaran H. Geometrically nonlinear transient analysis of moderately thick laminated composite shallow shells with generalized differential quadrature method. Compos Struct 2015;125:605–14. https://doi.org/10.1016/j.compstruct.2015.02.045.

[3] Yan T, Kitipornchai S, Yang J, He XQ. Dynamic behaviour of edge-cracked shear deformable functionally graded beams on an elastic foundation under a moving load. Compos Struct 2011;93(11):2992–3001. https://doi.org/10.1016/j.compstruct.2011.05.003.

[4] Foroutan R, Nemes J, Ghiasi H, Hubert P. Experimental investigation of high strain-rate behaviour of fabric composites. Compos Struct 2013;106:264–9. https://doi.org/10.1016/j.compstruct.2013.06.014.

[5] Priyanka P, Dixit A, Mali HS. High-strength hybrid textile composites with carbon, Kevlar, and E-glass fibers for impact-resistant structures. A review. Mech Compos Mater 2017;53:685–704. https://doi.org/10.1007/s11029-017-9696-2.

[6] Ari A, Bayram A, Karahan M, Karagöz S. Comparison of the mechanical properties of chopped glass, carbon, and aramid fiber reinforced polypropylene. Polym Polym Compos 2022;30:1–13. https://doi.org/10.1177/09673911221098570.

[7] Merlette TC, Diani J. Linear viscoelasticity of anisotropic carbon fibers reinforced thermoplastics: from micromechanics to dynamic torsion experiments. Compos B Eng 2025;290:111931. https://doi.org/10.1016/j.compositesb.2024.111931.

[8] Shariyat M, Jahangiri M. Nonlinear impact and damping investigations of viscoporoelastic functionally graded plates with in-plane diffusion and partial supports. Compos Struct 2020;245:112345. https://doi.org/10.1016/j.compstruct.2020.112345.

[9] Dojan CF, Ziaee M, Masoumipour A, Samuel J, Radosevich SJ, Yourdkhani M. Additive manufacturing of carbon fiber-reinforced thermoset composites via in-situ thermal curing. Nat Commun 2025;16:4691. https://doi.org/10.1038/s41467-025-59848-2.

[10] Lopez D, Thuillier S, Grohens Y. Prediction of elastic anisotropic thermo-dependent properties of discontinuous fiber-reinforced composites. J Compos Mater 2020;54(14):1913–23. https://doi.org/10.1177/0021998319889397.

[11] Li J, Durandet Y, Huang X, Sun G, Ruan D. Additively manufactured fiber-reinforced composites: a review of mechanical behavior and opportunities. J Mater Sci Technol 2022;119:219–44. https://doi.org/10.1016/j.jmst.2021.11.063.

[12] Parmiggiani A, Prato M, Pizzorni M. Effect of the fiber orientation on the tensile and flexural behavior of continuous carbon fiber composites made via fused filament fabrication. Int J Adv Manuf Technol 2021;114:2085–101. https://doi.org/10.1007/s00170-021-06997-5.

[13] Soori M, Jough FKG, Dastres R, Arezoo B. Additive manufacturing modification by artificial intelligence, machine learning, and deep learning: a review. Addit Manuf Front 2025;4(2):200198. https://doi.org/10.1016/j.amf.2025.200198.

[14] Tane M, Okuda H, Tanaka F. Nanocomposite microstructures dominating anisotropic elastic modulus in carbon fibers. Acta Mater 2019;166:75–84. https://doi.org/10.1016/j.actamat.2018.12.029.

[15] Smith RE. Ultrasonic elastic constants of carbon fibers and their composites. J Appl Phys 1972;43:2555–61. https://doi.org/10.1063/1.1661559.

[16] Sun Y, Zhao G, Yang F. Anisotropic behavior of the nanoindentation of single carbon fibers. Nanosci Nanotechnol Lett 2014;6:596–600. https://doi.org/10.1166/nnl.2014.1809.

[17] Csanádi T, Németh D, Zhang C, Dusza J. Nanoindentation derived elastic constants of carbon fibres and their nanostructural based predictions. Carbon 2017;119:314–25. https://doi.org/10.1016/j.carbon.2017.04.048.

[18] Oliver WC, Pharr GM. An improved technique for determining hardness and elastic modulus using load and displacement sensing indentation experiments. J Mater Res 1992;7:1564–83. https://doi.org/10.1557/JMR.1992.1564.

[19] Oliver WC, Pharr GM. Measurement of hardness and elastic modulus by instrumented indentation: advances in understanding and refinements to methodology. J Mater Res 2004;19:3–20. https://doi.org/10.1557/jmr.2004.19.1.3.

[20] Vlassak J, Nix W. Measuring the elastic properties of anisotropic materials by means of indentation experiments. J Mech Phys Solids 1997;42(8):1223–45. https://doi.org/10.1016/0022-5096(94)90033-7.

[21] Vlassak J, Nix W. Indentation modulus of elastically anisotropic half spaces. Philos Mag A Phys Condens Matter Struct Defects Mech Prop 1993;67(5):1045–56. https://doi.org/10.1080/01418619308224756.

[22] Shirasu K, Nagai C, Naito K. Mechanical anisotropy of PAN-based and pitch-based carbon fibers. Mech Eng J 2020;7(4):19–599. https://doi.org/10.1299/mej.19-00599.

[23] Shirasu K, Goto K, Naito K. Microstructure-elastic property relationships in carbon fibers: a nanoindentation study. Compos B Eng 2020;200:108342. https://doi.org/10.1016/j.compositesb.2020.108342.

[24] Goto K, Naito K, Shirasu K, Watanabe I. Numerical calculation and finite element analysis for anisotropic elastic properties of carbon fibers: dependence of integration subinterval and mesh size on indentation-derived elastic modulus. SN Appl Sci 2022;4:291. https://doi.org/10.1007/s42452-022-05183-w.

[25] Gonabadi H, Zamani Miandashti Z, Oila A. Micro-mechanical characterisation of 3D-printed composites via nano-indentation and finite-element homogenization techniques: overcoming challenges in orthotropic property measurement. Prog Addit Manuf 2025:108400. https://doi.org/10.1007/s40964-025-01131-3.

[26] Ballkoğlu F, Demircioğlu TK, Diler EA, Ataş A. Strain rate effect on the tensile properties of plain weave aramid, carbon, and glass fabric reinforced monolithic and hybrid composites. Inter J Mater Res 2022;113(6):587–98. https://doi.org/10.1515/ijmr-2021-8386.

[27] Choi JS, Choi H, Park SJ, Park MK. Comparative numerical evaluation for the low velocity impact behavior of T300 and T800 composite system. Carbon Lett 2017;22(1):89–95. https://doi.org/10.5714/CL.2017.22.089.

[28] Delafargue A, Ulm FJ. Explicit approximations of the indentation modulus of elastically orthotropic solids for conical indenters. Int J Solids Struct 2004;41:7351–560. https://doi.org/10.1016/j.ijsolstr.2004.06.019.

[29] Swadener JG, Pharr GM. Indentation of elastically anisotropic half-spaces by cones and parabolae of revolution. Philos Mag A Phys Condens Matter Struct Defects Mech Prop 2001;81(2):447–66. https://doi.org/10.1080/01418610108214314.

[30] Patel HR, Flood SH, Raju H, Tenorio MC, Pelegri AA. Nanoindentation of freestanding single kevlar® fibers with an adjusted indentation area function. J Mater Res Technol 2022;19:1472–83. https://doi.org/10.1016/j.jmrt.2022.05.065.

[31] Kube C. Elastic anisotropy of crystals. AIP Adv 2016;6:095209. https://doi.org/10.1063/1.4962996.

[32] Sanei SHR, Popescu D. 3d-printed carbon fiber reinforced polymer composites: a systematic review. J Compos Sci;4(3):98. https://doi.org/10.3390/jcs4030098.

[33] Huang ZM. On micromechanics approach to stiffness and strength of unidirectional composites. J Reinf Plast Compos 2019;38(4):167–96. https://doi.org/10.1177/0731684418811938.

[34] Wang H, Zhang H, Tang D, Goto K, Watanabe I, Kitazawa H, Kawai M, Mamiya H, Fujita D. Stress dependence of indentation modulus for carbon fiber in polymer composite. Sci Technol Adv Mater 2019;20(1):412–20. https://doi.org/10.1080/14686996.2019.1600202.